A PICTURE OF THE SPACE OF TYPICAL LEARNING TASKS

Anonymous authors
Paper under double-blind review

ABSTRACT

We develop a technique to analyze representations learned by deep networks when they are trained on different tasks using supervised, meta- and contrastive learning. We develop a technique to visualize such representations using an isometric embedding of the space of probabilistic models into a lower-dimensional space, i.e., one that preserves pairwise distances. We discover the following surprising phenomena that shed light upon the structure in the space of learning tasks: (1) the manifold of probabilistic models trained on different tasks using different representation learning methods is effectively low-dimensional; (2) supervised learning on one task results in a surprising amount of progress on seemingly dissimilar tasks; progress on other tasks is larger if the training task has diverse classes; (3) the structure of the space of tasks indicated by our analysis is consistent with parts of the Wordnet phylogenetic tree; (4) fine-tuning a model upon a sub-task does not change the representation much if the model was trained for a large number of epochs; (5) episodic meta-learning algorithms fit similar models eventually as that of supervised learning, even if the two traverse different trajectories during training; (6) contrastive learning methods trained on different datasets learn similar representations. We use classification tasks constructed from the CIFAR-10 and Imagenet datasets to study these phenomena.

1 INTRODUCTION

Exploiting data from related tasks to reduce the sample complexity of learning a desired task, is an idea that lies at the heart of burgeoning fields like transfer, multi-task, meta, few-shot, and self-supervised learning. These algorithms have shown an impressive ability to learn representations that can predict well on new tasks. The algorithms are very diverse in how they work but it stands to reason they must be exploiting some shared structure in the space of learning tasks. Although there is a large body of work that seeks to understand relatedness among tasks and how these algorithms exploit it (see §4), we do not know what this shared structure precisely is. Our work makes the following contributions to advancing this line of research.

We develop a technique to analyze the learned representation on a task, and its relationship to other tasks. Our key technical innovation is to use ideas from information geometry to characterize the geometry of the space of probabilistic models fit on different tasks. We develop methods to embed training trajectories of probabilistic models into a lower-dimensional space isometrically, i.e., while preserving pairwise distances. This allows us to faithfully visualize the geometry of these very high dimensional spaces (for Imagenet, our probabilistic models are in $\sim 10^7$ dimensions) and thereby interpret the geometry of the space of learning tasks. These technical tools are very general and shed light on the shared structure among tasks.

We point these technical tools to study how algorithms that learn from multiple tasks work. We provide evidence for the following phenomena.

(1) The manifold of probabilistic models trained on different tasks using different representation learning methods is effectively low-dimensional; and this dimensionality is rather small (for Imagenet, 10 dimensions capture 52% of the variance).
(2) Supervised learning on one task results in a surprising amount of progress on seemingly dissimilar tasks; progress on other tasks is larger if the training task has diverse classes;
(3) The structure of the space of tasks indicated by our analysis is consistent with parts of the Wordnet phylogenetic tree;
(4) Fine-tuning a model upon a sub-task does not change the representation much if the model was trained for a large number of epochs;

(5) Episodic meta-learning algorithms fit similar models eventually as that of supervised learning, even if the two traverse different trajectories during training;
(6) Contrastive learning methods trained on different datasets learn similar representations.

We demonstrate these findings on image classification tasks constructed from CIFAR-10 and Imagenet datasets.

2 Methods

Modeling the task We define a task P as a joint distribution on inputs $x \in \mathbb{R}^d$ and outputs $y \in \{1, \ldots, C\}$ corresponding to C classes. Suppose we have N independent and identically distributed samples $\{(x_n, y_n^*)\}_{n=1}^N$ from P. Let $\vec{y} = (y_1, \ldots, y_N)$ denote any sequence of outputs on these N samples and $\vec{y^*}$ denote the sequence of ground-truth labels. We may now model the task as

$$P_w(\vec{y}) = \prod_{n=1}^{N} p_w^n(y_n) \tag{1}$$

where w are the parameters of the model and we have used the shorthand $p_w^n(y_n) \equiv p_w(y_n \mid x_n)$. The true probability distribution which corresponds to the ground-truth labels is denoted by $P_* \equiv P(\vec{y^*})$. In the same way, let us denote by P_0 the probability distribution that corresponds to $p^n(y) = 1/C$ for all n and all y, i.e., P_0 predicts accurately on a fraction $1/C$ of the samples.

Bhattacharyya distance Given two models P_u and P_v parameterized by weights u and v respectively, we define the Bhattacharyya distance between them averaged over samples as

$$\begin{aligned} \mathrm{d_B}(P_u, P_v) &:= -N^{-1} \log \sum_{\vec{y}} \prod_n \sqrt{p_u(y_n)\, p_v(y_n)} \\ &\overset{(*)}{=} -N^{-1} \log \prod_{n=1}^{N} \sum_{c=1}^{C} \sqrt{p_u^n(c)\, p_v^n(c)} \\ &= -N^{-1} \sum_n \log \sum_c \sqrt{p_u^n(c)\, p_v^n(c)}; \end{aligned} \tag{2}$$

here $(*)$ follows because the samples are independent. Our model (1) involves a product over the probabilities of N samples. Typical distances for probability distributions, e.g., Hellinger distance $2N^{-1} \sum_n \left(1 - \sum_c \sqrt{p_u^n(c)\, p_v^n(c)}\right)$, saturate when the number of classes C is large (because random high-dimensional vectors are nearly orthogonal). It is thus difficult to use such distances to understand high-dimensional probabilistic models. However, the Bhattacharyya distance is well-behaved for large C due to the logarithm (Quinn et al., 2019), and that is why it is well suited to our problem.

Distances between trajectories of probabilistic models Consider a trajectory $(w(k))_{k=0,\ldots,T}$ that records the weights after T updates of the optimization algorithm, e.g., stochastic gradient descent. This trajectory corresponds to a trajectory of probabilistic models $\tilde{\tau}_w = (P_{w(k)})_{k=0,\ldots,T}$. We are interested in calculating distances between such training trajectories. First, consider $\tilde{\tau}_u = (u(0), u(1), u(2), \ldots, u(T))$ and another trajectory $\tilde{\tau}_v \equiv (u(0), u(2), u(4), \ldots, u(T), u(T), \ldots)$ which trains twice as fast but to the same end point. If we define the distance between these trajectories as, say, $\sum_k \mathrm{d_B}(P_{u(k)}, P_{v(k)})$, then the distance between $\tilde{\tau}_u$ and $\tilde{\tau}_v$ will be non-zero—even if they are fundamentally the same. This issue is more pronounced when we calculate distances between training trajectories of different tasks. It arises because we are recording each trajectory using a different time coordinate, namely its own training progress.

To compare two trajectories correctly, we need a notion of time that can allow us to uniquely index any trajectory. The geodesic between the start point P_0 and the true distribution P_* is a natural candidate for this purpose. Geodesics are locally length-minimizing curves in a metric space. For the product manifold in (1), we can obtain a closed-form formula for the geodesic as follows. We can think of the square root of the probabilities $\sqrt{p_u^n(c)}$ as a point on a C-dimensional sphere. Given two models P_u and P_v the geodesic connecting them under the Fisher information metric is the great circle on this sphere (Ito & Dechant, 2020, Eq. 47):

$$\sqrt{P_{u,v}^{\lambda}} = \frac{\sin\left((1-\lambda)\mathrm{d_G}\right)}{\sin\left(\mathrm{d_G}\right)} \sqrt{P_u} + \frac{\sin\left(\lambda \mathrm{d_G}\right)}{\sin\left(\mathrm{d_G}\right)} \sqrt{P_v}; \text{ for } \lambda \in [0, 1], \tag{3}$$

where $\mathrm{d_G} = \sum_n \cos^{-1}\left(\sum_c \sqrt{p_u^n(c)} \sqrt{p_v^n(c)}\right)$ is one half of the great-circle distance on the N-way product manifold of probability distributions $p_u^n(\cdot)$ and $p_v^n(\cdot)$. Every point w on the trajectory $\tilde{\tau}_w$ can

now be reindexed by a new time which we call "progress"

$$t_w = \inf_{\lambda \in [0,1]} \mathrm{d_G}(P_w, P^{\lambda}_{0,*}). \tag{4}$$

Note that the progress $t_w \in [0, 1]$ for any point on any trajectory. In practice, we solve (4) using bisection search (Brent, 1971). Observe that (3) also allows us to calculate the geodesic between two successive points $P_{w(k)}$ and $P_{w(k+1)}$ of the trajectory. Any point on this geodesic $P^{\lambda}_{w(k),w(k+1)}$ for $\lambda \in [0, 1]$ can be assigned a progress $t_{w(k)} + \lambda(t_{w(k+1)} - t_{w(k)})$. We have effectively converted our trajectory which is a discrete sequence of models $\tilde{\tau}_w = (P_{w(k)})_{k=0,\ldots,T}$ into a continuous curve $\tau_w = (P_{w(t)})_{t\in[0,1]}$. We can now calculate the distance between trajectories τ_u and τ_v as

$$\mathrm{d_{traj}}(\tau_u, \tau_v) = \int_0^1 \mathrm{d_B}(P_{u(t)}, P_{v(t)})\, \mathrm{d}t\,; \tag{5}$$

we approximate this integral in practice using a uniform grid on $[0, 1]$.

Riemann length of a trajectory of probabilistic models Divergences like the Bhattacharyya distance or the Kullback-Leibler (KL) distance (which is exactly the cross-entropy loss)

$$\mathrm{d_{KL}}(P_*, P_w) = -N^{-1} \sum_n \sum_c p^n_*(c) \log p^n_w(c) - H(P_*);$$

where $H(P_*)$ is the entropy of P_* (and independent of w) can be used to define a Riemannian structure in the space of probabilistic models (Amari, 2016). The distance between two models P_w and $P_{w+\mathrm{d}w}$ parametrized by infinitesimally different weights is

$$\mathrm{d}s^2 = 4\mathrm{d_B}(P_w, P_{w+\mathrm{d}w}) = \langle \mathrm{d}w\,, g(w)\,\mathrm{d}w\rangle + \mathcal{O}(\|\mathrm{d}w\|^2),$$

where $g(w) = N^{-1} \sum_{\bar{y}} (P_w)^{-1} \partial^2 P_w$ is the Fisher Information Matrix (FIM). This FIM is therefore the metric of the space of the probability distributions and weights w play the role of the coordinates in this space. The Bhattacharyya distance and the KL-divergence induce the same metric up to a scalar factor. We can therefore calculate the Riemann length of a trajectory τ_w by integrating the infinitesimal lengths

$$\mathrm{Length}(\tau_w) = 2 \int_0^1 \sqrt{\mathrm{d_B}(P_{w(t)}, P_{w(t+\mathrm{d}t)})}. \tag{6}$$

Observe that we do not need the FIM to calculate the length. We can think of the length of a trajectory taken by a model to reach the solution P_* compared to the length of the geodesic as a measure of the inefficiency of the training procedure. This inefficiency can arise because: (a) not all probability distributions along the geodesic can be parametrized by our model class (approximation error), and (b) the training process may take steps that are misaligned with the geodesic (e.g., due to the loss function, mini-batch updates, supervised vs. some other form of representation learning, etc.).

Mapping a model trained on one task to another task using "imprinting" We will consider different tasks $\{P^k\}_{k=1,\ldots,}$ with the same input domain but possibly different number of classes C^k. Given a model P^1_w parametrized by weights w for one task, we are interested in evaluating its learned representation on another task, say, P^2. There are many ways of doing so, e.g., one could fine-tune the weights using data from P^2. We use a simple technique that re-initializes the final layer of the model. Let us separate the weights into two parts $w = (w_1, w_2)$ for the backbone and the classifier respectively. Let $\varphi(x; w_1)$ denote the features of the penultimate layer corresponding to an input x. To clarify, the logits are given by $\mathbb{R}^{C^1} \ni {w_2}^\top \varphi(x; w_1)$ (with perhaps an added bias) and the output $p_w(c \mid x_n)$ for $c = 1, \ldots, C^1$ is computed using a softmax applied to these logits.

If we have learned w from one task P^1, then we can re-initialize each row of the classifier weights $(w_2)'_c$ for $c = 1, \ldots, C^2$ to maximize the cosine similarity with the average feature of samples from task P^2 with ground-truth class c:

$$(w_2)'_c = h/\|h\|_2 \quad \text{where } h = \textstyle\sum_{\{x:y^*_x=c\}} \varphi(x; w_1). \tag{7}$$

The new model $w = (w_1, {w_2}')$ can now be used to make predictions on the task P^2. This technique for mapping the learned representation from one task to another is motivated from previous work (Dhillon et al., 2020; Qi et al., 2018; Hu et al., 2015) which initializes the final layer of a model before adapting it to new classes using fine-tuning. It is called imprinting because rows of the classifier's weights can be thought of as templates of different classes against which features are compared.

Using imprinting, we can map a trajectory τ^1_w of a model being trained on task P^1 to another task P^2 by mapping each point along the trajectory; let us denote this mapped trajectory by $\tau^{1\to 2}_w$.

Remark 1 (Imprinting vs. training the final layer). We are interested in mapping 1000s of models across different trajectories to other tasks. Training the final layer for all these models is cumbersome and we can avoid doing so using imprinting. Note that if we were to train the classifier w_2 (with backbone w_1 fixed) using samples from the other task under the constraint that rows of w_2 have unit ℓ_2 norm, then we would obtain the imprinted weights as our solution.

How to choose an appropriate task to map different models to? Consider the training trajectory τ_u^1 of a model trained on task P^1 and another trajectory τ_v^2 of a model trained on task P^2. Using the procedure in (7), we can map these trajectories to the other task to get $\tau_u^{1\to 2}$ and $\tau_v^{2\to 1}$. This allows us to calculate $\mathrm{d}_{\text{traj}}(\tau_u^{1\to 2}, \tau_v^2)$ which is the distance of the trajectory of the model trained on P^1 and then mapped to P^2 with respect to the trajectory of a model trained on task P^2; we can calculate $\mathrm{d}_{\text{traj}}(\tau_v^{2\to 1}, \tau_u^1)$ analogously. Roughly speaking, if the two learning tasks P^1 and P^2 are very different, (e.g., Animals in CIFAR-10 and Vehicles in CIFAR-10), then these distances will be large.

The distances $\mathrm{d}_{\text{traj}}(\tau_u^{1\to 2}, \tau_v^2)$ and $\mathrm{d}_{\text{traj}}(\tau_v^{2\to 1}, \tau_u^1)$ are reasonable candidates to study similarities between tasks P^1 and P^2, but they are not equal to one another. We are also interested in doing such calculations with models trained on many different tasks, and mapping them to each other will lead to an explosion of quantities. To circumvent this, we map to a unique task whose output space is the union of the output spaces of the individual tasks, e.g., to study P^1 (Animals) and P^2 (Vehicles), we will map both trajectories to P^{U} which is all of CIFAR-10. We calculate quantities like

$$\mathrm{d}_{\text{traj}}(\tau_u^{1\to \mathrm{U}}, \tau_v^{2\to \mathrm{U}}). \tag{8}$$

Embedding a probabilistic model in lower-dimensions We use a technique called intensive principal component analysis (InPCA) (Quinn et al., 2019; Teoh et al., 2020) to embed a probabilistic model into a lower-dimensional space. This enables us to visually inspect relationships between different tasks and representation learning methods. For n probability distributions, consider a matrix $D \in \mathbb{R}^{n\times n}$ with entries $D_{uv} = \mathrm{d}_{\mathrm{B}}(P_u, P_v)$ and

$$W = -LDL/2 \tag{9}$$

where $L_{ij} = \delta_{ij} - 1/n$ is the centered version of D. An eigen-decomposition of $W = U\Sigma U^\top$ where the eigenvalues are sorted in descending order of their magnitudes $|\Sigma_{00}| \geq |\Sigma_{11}| \geq \ldots$ allows us to compute the embedding of these n probability distributions into an n-dimensional space as $\mathbb{R}^{n\times n} \ni X = U\sqrt{\Sigma}$. Unlike standard PCA where eigenvalues are non-negative, eigenvalues of InPCA can be both positive and negative. There are technical reasons for this (Quinn et al., 2019). But such an embedding into a Minkowski space allows the InPCA embedding to be an isometry:

$$\textstyle\sum_i \operatorname{sign}(\Sigma_{ii})\Sigma_{ii}^2 (X_u^i - X_v^i)^2 = \mathrm{d}_{\mathrm{B}}(P_u, P_v) \geq 0$$

for embeddings X_u, X_v of any two probability distributions P_u and P_v. In contrast, dimensionality reduction methods like t-SNE or UMAP preserve local pairwise distances but tend to distort global distances. A key benefit of isometry is that we will be able to visualize the geometric structure of the different probabilistic models, and by extension the tasks that they were fitted on, without it getting distorted—this cannot be done using non-isometric embeddings. We only use InPCA for visualization, all our findings are quantitative and do not rely on embedding into lower dimensions. Appendix A.2 describes how we implement InPCA for very high-dimensional probabilistic models.

3 Results

We next discuss our key results. Our experiments were conducted using multiple neural architectures and image-classification tasks created from the CIFAR-10 and Imagenet datasets; see Appendix A.

All the analysis in this paper (except Fig. 2) was conducted using the test data. All models were trained using the training data, but all mapped models, distances between trajectories, quantitative evaluation of progress and InPCA embeddings were computed using the test dataset. The reason for this is because we would to study the geometry of tasks as evidenced by samples that were not a part of training. To emphasize, we do not develop any new algorithms for learning in this paper and therefore using the test data to quantify relationships between tasks is reasonable; see similar motivations in Kaplun et al. (2022) among others. Our findings remain valid when training data is used for analysis; this is primarily because in most of our experiments, a representation is trained on one task but makes predictions on a completely new task after mapping.

Result 1. The manifold of models trained on different tasks, and using different representation learning methods, is effectively low-dimensional. We trained multiple models on 6 different

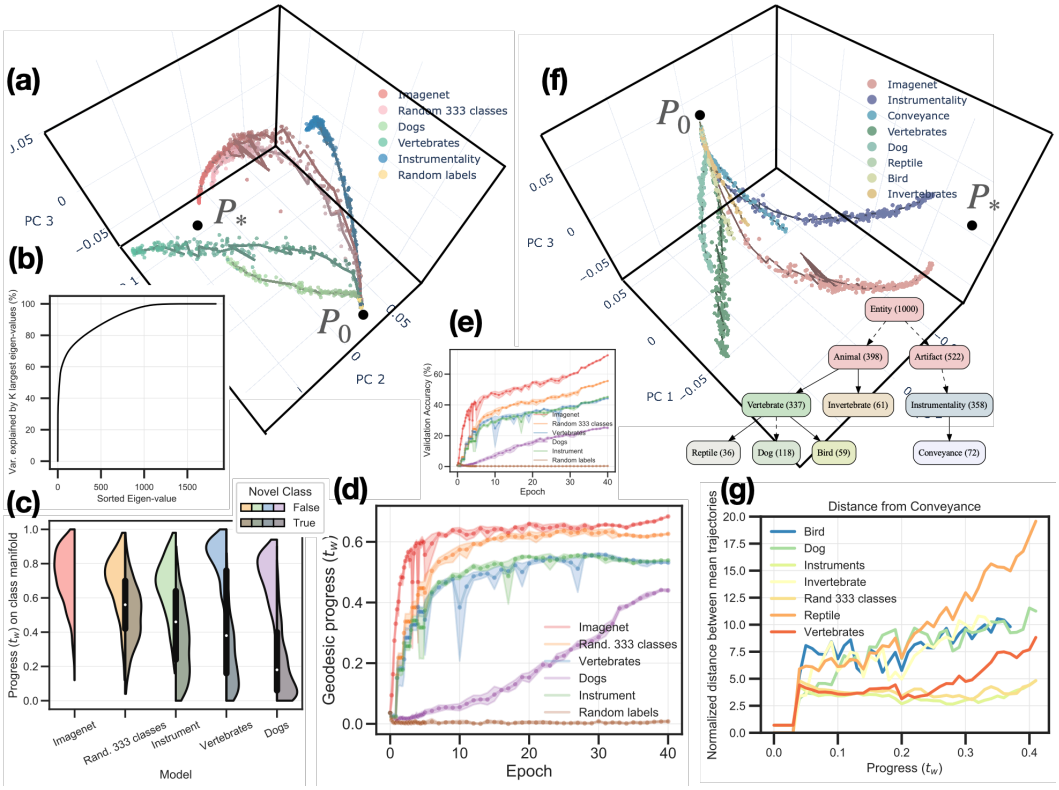

Figure 1: **(a)** InPCA embedding of training trajectories of probabilistic models trained on 6 tasks from Imagenet. Each point is one network, bold lines connect the averages of probabilities of 5 training trajectories of each task (5 random initializations in weight space). The point P_0 denotes start of training (complete ignorance) and P_* is drawn to show the model that predicts perfectly (truth). All trajectories move towards the end point of training on the entire Imagenet. Training on one task makes a remarkable amount of progress on unseen, seemingly dissimilar, classes. Trajectories of models trained on a random set of 333 classes are similar to those of the entire Imagenet. Some classes (Instrumentality) are closer to this trajectory while others such as Vertebrates and Dogs are farther away. Dogs is a semantic subset of Vertebrates; it splits at the beginning but seems to eventually reach a similar representation as one of the intermediate points of Vertebrates. See Result 1.

(b) Percentage variance captured by the subspace spanned by the top k InPCA eigenvectors. Top 10 dimensions capture more than 50% of the variance, and thus the manifold is effectively low-dimensional. See Result 1.

(c) If we train a model on Vertebrates, do we make progress on unseen classes? This plot measures the progress made by each model on classes seen during training (left half, lighter shade) and on novel classes (right half, darker shade). We compute t_w^c which is the progress t_w of images restricted to a single class c. This quantity t_w^c measures the quality of the representation for class c. The violin plots that denote the distribution of t_w^c indicate that we make more progress on classes seen during training. If the model sees a larger diversity of classes (like with random 333 classes), more progress is made on the novel classes. Surprisingly, even if we train on just the "Dogs", we make some progress on novel classes.

(d) Progress t_w (4) on the Y-axis against the number of epochs of training on the X-axis. The progress t_w increases with more epochs of training—all models make non-trivial progress towards the truth P_* ($t_w = 1$). Surprisingly, even if we train on only Dogs (118 classes) we make progress on the entire Imagenet. **(e)** Progress is strongly correlated with accuracy. See Result 2.

(f) Trajectories of models trained on different phyla of Wordnet (colors match those of the inset graph). The model manifold is again effectively low-dimensional (31% explained variance in 3 dimensions). Trajectories of tasks that are nearby in Wordnet are also nearby, and vice-versa. **(g)** plots the Bhattacharya distance between the mean trajectories (over random initializations) on different tasks and the mean trajectory of Conveyance. This distance is normalized by the average of the tube radii (maximum distance of one of the 5 trajectories from the mean, computed at each progress) of the two trajectories. Such quantities allow us to make precise statements about the differences between representations and show some very surprising conclusions. E.g., trajectories of random 333 classes (light orange) are closer to Conveyance (as expected), but those of Vertebrates (red) are equally far away for more than 60% ($t_w \approx 0.25$) of the progress. In other words, training on Vertebrates (reptiles, dog, bird) makes a remarkable progress on Conveyance (cars, planes). See Result 2.

sub-tasks of Imagenet (from 5 random initializations each) to study the dimensionality of the manifold of probabilistic models along the training trajectories (100 points equidistant in progress (4)) after mapping all models to all Imagenet classes ($\sim 10^8$ dimensions). The first 3 dimensions of InPCA (Fig. 1a) capture 33% of the variance (Fig. 1b shows more eigenvalues). This is a remarkably low-dimensional manifold. It is not exactly low-dimensional because the explained variance is not 1, but it is an effectively low-dimensional manifold. Observe that this experiment also indicates that the individual manifolds of models trained on one task are low-dimensional, even if they start from different random initializations in the weight space. Such low-dimensional manifolds are seen in *all* our experiments, irrespective of the specific method used for representation learning, namely, supervised, transfer (fine-tuning), meta and contrastive learning.

Result 2. Supervised learning on one task results in a surprising amount of progress on seemingly dissimilar tasks. Progress on other tasks is larger if the training task has diverse classes. We studied the progress t_w (4) made by models (Fig. 1d) trained on tasks from Result 1. Training on the task "Dogs" makes progress on other tasks, even seemingly dissimilar ones like "Instruments" (which contains vehicles, devices and clothing). In fact, it makes progress on the entire Imagenet (about 63.38% of the progress of a model trained directly on Imagenet). Progress is larger for larger phyla of Imagenet (Vertebrates and Instruments). But what is surprising is that if we train on a random subset of 333 classes (a third of Imagenet), then the progress on the entire Imagenet is very large (92%). This points to a remarkably strong shared structure among classes even for rich datasets such as Imagenet. Note that this *does not* mean that tasks such as Vertebrates and Instruments are similar to each other. Even if training trajectories are similar for a while, they do bifurcate eventually and the final models are different (Fig. 1g).

To study this further, we projected models trained on one task onto the geodesics of unseen classes (Fig. 1c) calculated using (3)). A model trained on the entire Imagenet makes uneven progress on the various classes (but about $t_w = 0.8$ progress across them, progress is highly correlated with test error of different classes). Models trained on the 6 individual tasks also make progress on other unseen classes. As before, training on Instruments, Vertebrates, Dogs makes smaller progress on unseen classes compared to training on a random subset of 333 classes. This is geometric evidence of the widely noticed (and exploited) phenomenon that the more diverse the training dataset, the better the generalization to *unseen* classes/tasks.

Result 3. The structure of the space of tasks indicated by our visualization technique is consistent with parts of the Wordnet phylogenetic tree To obtain a more fine-grained characterization of how the geometry in the space of learning tasks reflects the semantics of tasks, we selected two particular phyla of Imagenet (Animals, Artifacts) and created sub-tasks using classes that belong to these phyla (Fig. 1f). Trajectories of models trained on Instruments and Conveyance are closer together than those of Animals. Within the Animals phylum, trajectories of Vertebrates (Dog, Reptile, Bird) are closer together than those of Invertebrates (Fig. 1g for quantitative metrics). Effectively, we can recover a part of the phylogenetic tree of Wordnet using our training trajectories. We speculate that this may point to some shared structure between visual features of images and natural language-based semantics (which was used to create Wordnet (Miller, 1998)) of the corresponding categories. This alignment with a natural notion of relatedness also demonstrates the effectiveness of our methods.

Result 4. Fine-tuning a pre-trained model on a sub-task does not change the representation much. To understand how models train on multiple tasks, we selected two binary classification sub-tasks of CIFAR-10 (Airplane vs. Automobile, and Bird vs. Cat). We selected models at different stages of standard supervised learning on CIFAR-10 (i.e., using 10-way output and softmax cross-entropy loss) and fine-tuned each of these models on two sub-tasks (the entire network is fine-tuned without freezing the backbone). As the adjoining figure shows, models that were fine-tuned from earlier parts of the trajectory travel a large distance and move away from trajectories of the supervised learned CIFAR-10 models. As we fine-tune later and later models, the distance traveled away from the trajectory is smaller and smaller, i.e., changes in the representation are smaller. For a fully-trained CIFAR-10 model which interpolates the training data, the distance traveled by fine-tuning is very small (the points are almost indistinguishable in the picture); this is because both P^1 and P^2 are subsets of CIFAR-10.

Algorithms for transfer learning train on a source task before fine-tuning the model on the target task. If two tasks share a large part of their training trajectory, then we may start the fine-tuning from many shared intermediate points. If the chosen point is farther along in terms of progress then the efficiency resulting from using the source task is higher because the trajectory required to fit the

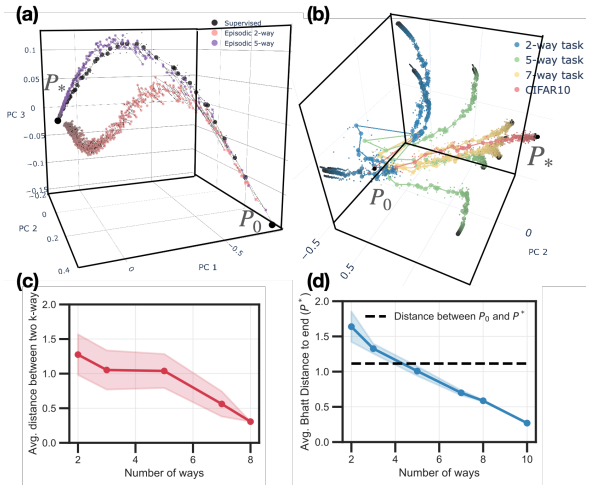

Figure 2: **(a)** Training trajectories for supervised learning (black), 2-way (pink) and 5-way episodic meta-learning (purple). Trajectories of 5-way meta-learning are very similar to those of supervised learning and eventually reach very similar models and high test accuracy. In contrast, 2-way meta-learning has a much longer trajectory (about 40× longer in Riemann length than black) and does not reach a good test accuracy (on all 10 CIFAR-10 classes). Representations are similar during early parts of training even if these are quite different learning mechanisms. **(b)** Trajectories of 2-way (blue), 5-way (green), 7-way (yellow) meta-learning compared to supervised learning (red). For large "way", trajectories are similar to supervised learning but they deviate from the red trajectories quickly for small ways. **(c)** Average distance between two k-way meta-learning trajectories decreases with k, this is a geometric evidence of the variance of predictions of learned representations. **(d)** Training with a small way leads to models that predict poorly on test data (large distances from truth). **These embeddings were calculated using the training dataset. The rationale being that we wanted to show how different meta-learning and supervised learning are during training.**

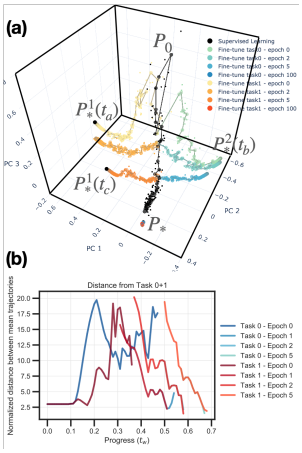

Figure 3: **(a)** Fine-tuning trajectories on Airplane vs. Automobile, and Bird vs. Cat sub-tasks of CIFAR-10 (warm and cold hues) pre-trained from different points along the trajectory of supervised learning. If the pretrained model has progressed further towards the truth P_*, then fine-tuning it on a subtask does not change the representation much. The final trajectory (fine-tuning from epoch 100) is indistinguishable from P_*. **(b)** Bhattacharya distance between the mean trajectories normalized by the average of the tube radii (like Fig. 1g). Models (say, fine-tuned after Epoch 5 on Task 1) go *backwards* in progress, i.e., they unlearn the pretrained representation in order to fit the new task. This occurs as early as Epoch 1 here. It suggests that learning occurs extremely rapidly at the beginning and determines the efficiency of fine-tuning. Some curves here are not visible because they are overlapping heavily.

target task is shorter; such trajectories were used in (Gao & Chaudhari, 2021) to define a distance between tasks. As we saw in Result 2, trajectories of different tasks bifurcate after a shared part. The resultant deviation less for related tasks and more for dissimilar tasks (Fig. 3a, Fig. 1a,f). Therefore it is difficult to know *a priori* from which point one should start the fine-tuning from without knowing the manifold of the target task. In particular, our geometric picture indicates that fine-tuning from a fully-trained model can be detrimental to the accuracy on the target task. This has been noticed in a number of places in the transfer learning literature, e.g., Li et al. (2020), and has also been studied theoretically (Gao & Chaudhari, 2020).

Result 5. Episodic meta-learning algorithms fit a similar model eventually as that of supervised learning, even if the two traverse very different trajectories during training. Meta-learning methods build a representation which can be adapted to a new task (Thrun & Pratt, 2012). We studied a common variant, the so-called episodic training methods (Bengio et al., 1992), through the perspective of few-shot learning (Vinyals et al., 2016). In these methods, each mini-batch consists of samples from C^w classes (called "way", chosen randomly out of the C classes) split into two parts: a "support set" D_s of s samples/class (called "shot"), and a "query set" D_q of q samples/class. Typical methods, say prototypical networks of Snell et al. (2017b), implement a clustering loss on features of the query samples using the averaged features of the support samples $\varphi_c = s^{-1} \sum_{\{x \in D_s, y^*(x)=c\}} \varphi(x; w_1)$ for all $c = 1, \ldots, C^w$ as the cluster centroids. This involves maximizing the likelihood

$$\forall x \in D_q, \text{ if } y^*(x) = c : p(\varphi(x; w_1)) \propto \exp\left(-\|\varphi_c - \varphi(x; w_1)\|^2/2\right) \tag{10}$$

over query samples. If features φ lie on an ℓ_2 ball of radius 1, then maximizing this likelihood is akin to maximizing the cosine similarity between cluster centroids computed from the support samples and features of the query samples. At the end of training, the same clustering loss with the learned backbone w_1 is used to predict on unseen classes (using "few" support samples to compute centroids).

We compared trajectories of episodic meta-learning to the trajectory taken by supervised learning using the cross-entropy loss over all C classes in Fig. 2. Episodic meta-learning methods are quite different from supervised learning so it seems surprising that both arrive at the same solution Fig. 2a,b. But this is consistent with recent literature which has noticed that the performance of few-shot learning methods using supervised learning (followed by fine-tuning) is comparable to or better than episodic meta-learning (Dhillon et al., 2020; Kolesnikov et al., 2020; Fakoor et al., 2020). The supervised learned representation also minimizes the clustering loss (10). We find that the trajectory length of episodic training is about 40$\times$ longer than that of supervised learning.

Few-shot accuracy of episodic training is better with a large way (Gidaris & Komodakis, 2018). We trained models with different ways to study this (Fig. 2b). We find that the radius of the tube that encapsulates the models of 2-way meta-learning around their mean trajectory is very large, almost as large as the total length of the trajectory, i.e., different models trained with a small way learn very different representations. Tube radius decreases as the way increases (Fig. 2c). Further, the distance of models from the truth P_* (which is close to the end point of the supervised learning model) is higher for a small way (Fig. 2d). This is geometric evidence of the widely used empirical practice of using a large number of way in episodic meta-learning. Observe that as the way increases, the trajectory of the episodic meta-learning becomes more and more similar to that of supervised learning.

Result 6. Contrastive learning methods trained on different datasets learn similar representations. Contrastive learning (Becker & Hinton, 1992) learns representations without using ground-truth labels (Gutmann & Hyvärinen, 2010; Chen et al., 2020a). It has been extremely effective for self-supervised learning (Doersch & Zisserman, 2017; Kolesnikov et al., 2019), e.g., prediction accuracy with 1–10% labeled data is close to that of supervised learning using all data (Chen et al., 2020b). We compared representations learned using contrastive learning with those from supervised learning to understand some aspects of why the former are so effective.

Consider a task P and a set of augmentations G (e.g., cropping, resizing, blurring, color/contrast/brightness distortion etc.). Given inputs (say images) x from P, contrastive learning forces the representation $\varphi(g(x); w_1)$ and $\varphi(g'(x); w_1)$ (shortened to $\varphi(g(x))$ below) of the same input for two different augmentations g, g' to be similar. And forces it to be different from representations of other augmented inputs x' (Zbontar et al., 2021; Bachman et al., 2019; Dosovitskiy et al., 2014).

We used a popular method called SimCLR (Chen et al., 2020a) to perform contrastive learning on images from four sets of classes (airplane-automobile, bird-cat, ship-truck) and all of CIFAR-10. We compared the learned representation to that from supervised learning on two tasks (airplane-automobile and all of CIFAR-10). Models trained using contrastive learning on two-class datasets learn very different representations from models trained on the same task but using supervised learning. Models trained using contrastive learning on different datasets learning similar representations (trajectories of all three two-class datasets are very close to each other). This is reasonable because contrastive learning does not use any information from the labels. It is surprising however that the trajectory of models from contrastive learning on these two-class datasets is similar to trajectories of models from contrastive learning on the entire CIFAR-10.

4 Related Work and Discussion

Understanding the space of learning tasks. A large body of work has sought to characterize relationships between learning tasks, e.g., domain specific methods (Zamir et al., 2018; Cui et al., 2018; Pennington et al., 2014), learning theoretic work (Baxter, 2000; Maurer, 2006; Ben-David et al., 2010; Ramesh & Chaudhari, 2022; Tripuraneni et al., 2020; Hanneke & Kpotufe, 2020; Caruana, 1997), and information-theoretic analyses (Jaakkola & Haussler, 1999; Achille et al., 2019a;b). Broadly speaking, this work has focused on understanding the accuracy of a model on a new task when it is trained upon a related task, e.g., relationships between tasks are characterized using the excess risk of a hypothesis.

Like these above works, our methods also allow us to say things like "task P^1 is far from P^2 as compared to P^3". But we heavily exploit information geometry and can go much further. Our methods shed light on the geometric structure in the space of tasks using the geometry of probabilistic models of these tasks. This allows us to make quantitative conclusions such as "the divergence

between P^1 and P^2 eventually is more than that of P^1 and P^3, but representations learned on these tasks are similar for 30% of the way". Therefore our methods allow us to paint a picture of the space of the tasks that is quantitative and globally consistent.

There is strong structure in typical inputs, e.g., recent work on understanding generalization (Yang et al., 2022; Bartlett et al., 2020) as well as older work such as (Simoncelli & Olshausen, 2001; Field, 1994; Marr, 2010) has argued that visual data is effectively low-dimensional. Our works suggests that tasks also share a low-dimensional structure. Just like the effective low-dimensionality of inputs enables generalization on one task, effective low-dimensionality of the manifold of models trained on different tasks could perhaps explain generalization to new tasks.

Relationships between tasks in computational neuroscience. Our results are conceptually close to those on organization and representation of semantic knowledge (Mandler & McDonough, 1993). Such work has primarily used simple theoretical models, e.g., linear dynamics of Saxe et al. (2019) (who also use MDS). Our tools are very general and paint a similar picture of ontologies of complex tasks. There is some resemblance in how our different networks learn the task in a similar fashion (low-dimensional manifold, trajectories across different random seeds and similar tasks are very close to each other), and how different individuals share the same notion of what constitutes a task (Rosch & Mervis, 1975). Concept formalization and specialization over age (Vosniadou & Brewer, 1992) also resembles our experiment in how fine-tuning models trained for longer periods changes the representation marginally. Our goals are similar to those of works like Sorscher et al. (2021) but our focus is very different. We have focused our techniques on studying how representation learning on multiple tasks works.

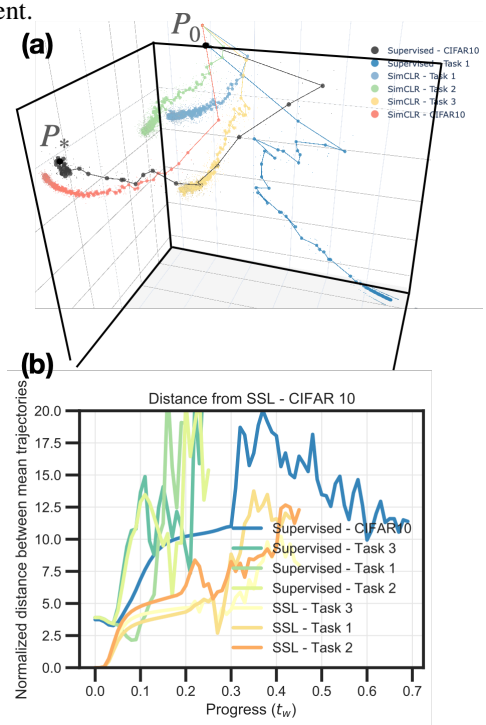

Figure 4: **(a)** Trajectories of contrastive learning (SimCLR) on 3 datasets (two classes each) and entire CIFAR-10 compared to those of supervised learning. SimCLR on entire CIFAR-10 learns a similar representation as that of the supervised learned model P_* (which fits the training data perfectly). SimCLR trajectories are close to each other even if different datasets were used to train them. It may seem from the embedding that SimCLR trajectories are similar to that supervised learning, which would be very surprising because the former does not use any labels, but see below.
(b) Bhattacharyya distance between the mean trajectories of all models and the mean trajectory of SimCLR on all CIFAR-10. This distance is normalized by the average of the tube radii (like Fig. 1g). SimCLR trajectories are indeed very close to each other (mean distance is $\sim 5\times$ more than their tube radii for about 45% of the way ($t_w \approx 0.2$)). In contrast to (a), this plot indicates that SimCLR trajectories are much farther away from the supervised learning trajectory (blue) than they are to SimCLR on CIFAR-10.

Visualizing training trajectories of deep networks. A large number of works have investigated trajectories of deep networks and the energy landscape during or after training using dimensionality reduction techniques (Horoi et al., 2021; Li et al., 2018; Huang et al., 2020). The key distinction with respect to this existing work—and our key technical innovation—is that we visualize the function space, not the weight space. We study the function space of deep networks by evaluating the underlying probabilistic model on finite samples. While the weight space has symmetries (Freeman & Bruna, 2017; Garipov et al., 2018) and nontrivial dynamics (Tanaka & Kunin, 2021; Chaudhari & Soatto, 2018), the function space, i.e,. our large vector $[0,1]^{N\times C} \ni \{p_w(c \mid x_i)\}$ completely characterizes the output of the model. In comparison, the loss or the error which are typically used to reason about relationships between tasks, are very coarse summaries of the predictions. Any two models trained on the same task can be rigorously studied in our "finite-dimensional function space" to understand their predictions. Another key innovation is that our mapping procedure allows us to study the representation of the penultimate layer of any two models, even if they were trained on different tasks.

References

Achille, Alessandro and Lam, Michael and Tewari, Rahul and Ravichandran, Avinash and Maji, Subhransu and Fowlkes, Charless C and Soatto, Stefano and Perona, Pietro. Task2vec: Task embedding for meta-learning. In *Proceedings of the IEEE International Conference on Computer Vision*, pp. 6430–6439, 2019a.

Achille, Alessandro and Mbeng, Glen and Soatto, Stefano. Dynamics and Reachability of Learning Tasks. *arXiv:1810.02440 [cs, stat]*, May 2019b.

Shun-ichi Amari. *Information Geometry and Its Applications*, volume 194 of *Applied Mathematical Sciences*. Tokyo, 2016.

Bachman, Philip and Hjelm, R Devon and Buchwalter, William. Learning representations by maximizing mutual information across views. *Advances in neural information processing systems*, 32, 2019.

Bartlett, Peter L and Long, Philip M and Lugosi, Gábor and Tsigler, Alexander. Benign overfitting in linear regression. *Proceedings of the National Academy of Sciences*, 117(48):30063–30070, 2020.

Baxter, Jonathan. A model of inductive bias learning. *Journal of artificial intelligence research*, 12: 149–198, 2000.

Becker, Suzanna and Hinton, Geoffrey E. Self-organizing neural network that discovers surfaces in random-dot stereograms. *Nature*, 355(6356):161–163, 1992.

Ben-David, Shai and Blitzer, John and Crammer, Koby and Kulesza, Alex and Pereira, Fernando and Vaughan, Jennifer Wortman. A theory of learning from different domains. *Machine learning*, 79 (1):151–175, 2010.

Bengio, Samy and Bengio, Yoshua and Cloutier, Jocelyn and Gecsei, Jan. On the optimization of a synaptic learning rule. In *Preprints Conf. Optimality in Artificial and Biological Neural Networks*, pp. 6–8, 1992.

Brent, Richard P. An algorithm with guaranteed convergence for finding a zero of a function. *The computer journal*, 14(4):422–425, 1971.

Caruana, Rich. Multitask learning. *Machine learning*, 28(1):41–75, 1997.

Chaudhari, Pratik and Soatto, Stefano. Stochastic gradient descent performs variational inference, converges to limit cycles for deep networks. *ICLR*, 2018.

Chen, Ting and Kornblith, Simon and Norouzi, Mohammad and Hinton, Geoffrey. A simple framework for contrastive learning of visual representations. In *International Conference on Machine Learning*, pp. 1597–1607, 2020a.

Chen, Ting and Kornblith, Simon and Swersky, Kevin and Norouzi, Mohammad and Hinton, Geoffrey E. Big self-supervised models are strong semi-supervised learners. *Advances in neural information processing systems*, 33:22243–22255, 2020b.

Cui, Yin and Song, Yang and Sun, Chen and Howard, Andrew and Belongie, Serge. Large scale fine-grained categorization and domain-specific transfer learning. In *Proceedings of the IEEE Conference on Computer Vision and Pattern Recognition*, pp. 4109–4118, 2018.

Deng, Jia and Dong, Wei and Socher, Richard and Li, Li-Jia and Li, Kai and Fei-Fei, Li. Imagenet: A large-scale hierarchical image database. In *2009 IEEE Conference on Computer Vision and Pattern Recognition*, pp. 248–255, 2009.

Dhillon, Guneet S and Chaudhari, Pratik and Ravichandran, Avinash and Soatto, Stefano. A baseline for few-shot image classification. In *ICLR*, 2020.

Doersch, Carl and Zisserman, Andrew. Multi-task self-supervised visual learning. In *Proceedings of the IEEE international conference on computer vision*, pp. 2051–2060, 2017.

Dosovitskiy, Alexey and Springenberg, Jost Tobias and Riedmiller, Martin and Brox, Thomas. Discriminative unsupervised feature learning with convolutional neural networks. *Advances in neural information processing systems*, 27, 2014.

Fakoor, Rasool and Chaudhari, Pratik and Soatto, Stefano and Smola, Alexander J. Meta-Q-Learning. In *ICLR*, 2020.

Field, David J. What is the goal of sensory coding? *Neural computation*, 6(4):559–601, 1994.

Freeman, C Daniel and Bruna, Joan. Topology and geometry of half-rectified network optimization. In *ICLR*, 2017.

Gao, Yansong and Chaudhari, Pratik. A free-energy principle for representation learning. In *Proc. of International Conference of Machine Learning (ICML)*, 2020.

Gao, Yansong and Chaudhari, Pratik. An information-geometric distance on the space of tasks. In *ICML*, 2021.

Garipov, Timur and Izmailov, Pavel and Podoprikhin, Dmitrii and Vetrov, Dmitry and Wilson, Andrew Gordon. Loss surfaces, mode connectivity, and fast ensembling of dnns. In *Proceedings of the 32nd International Conference on Neural Information Processing Systems*, pp. 8803–8812, 2018.

Gidaris, Spyros and Komodakis, Nikos. Dynamic few-shot visual learning without forgetting. In *Proceedings of the IEEE Conference on Computer Vision and Pattern Recognition*, pp. 4367–4375, 2018.

Gutmann, Michael and Hyvärinen, Aapo. Noise-contrastive estimation: A new estimation principle for unnormalized statistical models. In *Proceedings of the thirteenth international conference on artificial intelligence and statistics*, pp. 297–304. JMLR Workshop and Conference Proceedings, 2010.

Hanneke, Steve and Kpotufe, Samory. A no-free-lunch theorem for multitask learning. *arXiv preprint arXiv:2006.15785*, 2020.

He, Kaiming and Zhang, Xiangyu and Ren, Shaoqing and Sun, Jian. Deep residual learning for image recognition. In *Proceedings of the IEEE Conference on Computer Vision and Pattern Recognition*, pp. 770–778, 2016.

Horoi, Stefan and Huang, Jessie and Wolf, Guy and Krishnaswamy, Smita. Visualizing high-dimensional trajectories on the loss-landscape of ANNs. *arXiv preprint arXiv:2102.00485*, 2021.

Hu, Junlin and Lu, Jiwen and Tan, Yap-Peng. Deep transfer metric learning. In *Proceedings of the IEEE Conference on Computer Vision and Pattern Recognition*, pp. 325–333, 2015.

Huang, W Ronny and Emam, Zeyad and Goldblum, Micah and Fowl, Liam and Terry, Justin K and Huang, Furong and Goldstein, Tom. Understanding generalization through visualizations. 2020.

Ito, Sosuke and Dechant, Andreas. Stochastic time evolution, information geometry, and the Cramér-Rao bound. *Physical Review X*, 10(2):021056, 2020.

Jaakkola, Tommi and Haussler, David. Exploiting generative models in discriminative classifiers. In *Advances in Neural Information Processing Systems*, pp. 487–493, 1999.

Kaplun, Gal and Ghosh, Nikhil and Garg, Saurabh and Barak, Boaz and Nakkiran, Preetum. Deconstructing distributions: A pointwise framework of learning. *arXiv preprint arXiv:2202.09931*, 2022.

Kolesnikov, Alexander and Zhai, Xiaohua and Beyer, Lucas. Revisiting self-supervised visual representation learning. In *Proceedings of the IEEE/CVF conference on computer vision and pattern recognition*, pp. 1920–1929, 2019.

Kolesnikov, Alexander and Beyer, Lucas and Zhai, Xiaohua and Puigcerver, Joan and Yung, Jessica and Gelly, Sylvain and Houlsby, Neil. Big Transfer (BiT): General Visual Representation Learning. *arXiv:1912.11370 [cs]*, May 2020.

Krizhevsky, A. *Learning Multiple Layers of Features from Tiny Images*. PhD thesis, Computer Science, University of Toronto, 2009.

Guillaume Leclerc and Andrew Ilyas and Logan Engstrom and Sung Min Park and Hadi Salman and Aleksander Madry. ffcv. https://github.com/libffcv/ffcv/, 2022.

Li, Hao and Xu, Zheng and Taylor, Gavin and Goldstein, Tom. Visualizing the loss landscape of neural nets. In *ICLR*, 2018.

Li, Hao and Chaudhari, Pratik and Yang, Hao and Lam, Michael and Ravichandran, Avinash and Bhotika, Rahul and Soatto, Stefano. Rethinking the hyper-parameters for fine-tuning. In *Proc. of International Conference of Learning and Representations (ICLR)*, 2020.

Mandler, Jean M and McDonough, Laraine. Concept formation in infancy. *Cognitive development*, 8 (3):291–318, 1993.

David Marr. *Vision: A Computational Investigation into the Human Representation and Processing of Visual Information*. 2010.

Maurer, Andreas. Bounds for linear multi-task learning. *The Journal of Machine Learning Research*, 7:117–139, 2006.

George A Miller. *WordNet: An Electronic Lexical Database*. 1998.

Nielsen, Frank and Boltz, Sylvain. The burbea-rao and bhattacharyya centroids. *IEEE Transactions on Information Theory*, 57(8):5455–5466, 2011.

Pennington, Jeffrey and Socher, Richard and Manning, Christopher D. Glove: Global vectors for word representation. In *Proceedings of the 2014 Conference on Empirical Methods in Natural Language Processing (EMNLP)*, pp. 1532–1543, 2014.

Qi, Hang and Brown, Matthew and Lowe, David G. Low-shot learning with imprinted weights. In *Proceedings of the IEEE Conference on Computer Vision and Pattern Recognition*, pp. 5822–5830, 2018.

Quinn, Katherine N and Clement, Colin B and De Bernardis, Francesco and Niemack, Michael D and Sethna, James P. Visualizing probabilistic models and data with intensive principal component analysis. *Proceedings of the National Academy of Sciences*, 116(28):13762–13767, 2019.

Ramesh, Rahul and Chaudhari, Pratik. Model Zoo: A Growing "Brain" That Learns Continually. In *ICLR*, 2022.

Rosch, Eleanor and Mervis, Carolyn B. Family resemblances: Studies in the internal structure of categories. *Cognitive psychology*, 7(4):573–605, 1975.

Saxe, Andrew M and McClelland, James L and Ganguli, Surya. A mathematical theory of semantic development in deep neural networks. *Proceedings of the National Academy of Sciences*, 116(23): 11537–11546, 2019.

Simoncelli, Eero P and Olshausen, Bruno A. Natural image statistics and neural representation. *Annual review of neuroscience*, 24(1):1193–1216, 2001.

Snell, Jake and Swersky, Kevin and Zemel, Richard. Prototypical networks for few-shot learning. In *Proceedings of the 31st International Conference on Neural Information Processing Systems*, pp. 4080–4090, 2017a.

Snell, Jake and Swersky, Kevin and Zemel, Richard. Prototypical networks for few-shot learning. In *Advances in Neural Information Processing Systems*, pp. 4077–4087, 2017b.

Sorscher, Ben and Ganguli, Surya and Sompolinsky, Haim. The geometry of concept learning. *bioRxiv : the preprint server for biology*, 2021.

Tanaka, Hidenori and Kunin, Daniel. Noether's learning dynamics: The role of kinetic symmetry breaking in deep learning. *arXiv preprint arXiv:2105.02716*, 2021.

Teoh, Han Kheng and Quinn, Katherine N. and Kent-Dobias, Jaron and Clement, Colin B. and Xu, Qingyang and Sethna, James P. Visualizing probabilistic models in Minkowski space with intensive symmetrized Kullback-Leibler embedding. *Physical Review Research*, 2(3):033221, August 2020.

Sebastian Thrun and Lorien Pratt. *Learning to Learn*. 2012.

Tripuraneni, Nilesh and Jin, Chi and Jordan, Michael I. Provable meta-learning of linear representations. *arXiv preprint arXiv:2002.11684*, 2020.

Vinyals, Oriol and Blundell, Charles and Lillicrap, Timothy and Wierstra, Daan and others. Matching networks for one shot learning. In *Advances in Neural Information Processing Systems*, pp. 3630–3638, 2016.

Vosniadou, Stella and Brewer, William F. Mental models of the earth: A study of conceptual change in childhood. *Cognitive psychology*, 24(4):535–585, 1992.

Yang, Rubing and Mao, Jialin and Chaudhari, Pratik. Does the data induce capacity control in deep learning? In *ICML*, 2022.

Zagoruyko, Sergey and Komodakis, Nikos. Wide residual networks. In *British Machine Vision Conference 2016*, 2016.

Zamir, Amir R and Sax, Alexander and Shen, William and Guibas, Leonidas J and Malik, Jitendra and Savarese, Silvio. Taskonomy: Disentangling task transfer learning. In *Proceedings of the IEEE Conference on Computer Vision and Pattern Recognition*, pp. 3712–3722, 2018.

Zbontar, Jure and Jing, Li and Misra, Ishan and LeCun, Yann and Deny, Stéphane. Barlow twins: Self-supervised learning via redundancy reduction. In *International Conference on Machine Learning*, pp. 12310–12320, 2021.

Zhang, Richard. Making convolutional networks shift-invariant again. In *International conference on machine learning*, pp. 7324–7334. PMLR, 2019.

A Details of the experimental setup

Data
We performed experiments using two datasets.

1. CIFAR10 (Krizhevsky, 2009) has 10 classes (airplane, automobile, bird, cat, deer, dog, frog, horse, ship, truck) with RGB images of size 32×32, and
2. Imagenet (Deng et al., 2009) has 1000 classes each with about 1000 RGB images of size 224×224.

Architectures We use a Wide-Resnet (Zagoruyko & Komodakis, 2016) architecture for supervised learning experiments on CIFAR-10 (WRN-16-4 with depth 16 and widening factor of 4) and a Resnet-18 (He et al., 2016) to train a model using SimCLR. All experiments on Imagenet use the Resnet-50 architecture.

All convolutional layers are initialized using the Kaiming-Normal initialization. For the Wide-Resnet, the final pooling layer is replaced with an adaptive pooling layer in order to handle input images of different sizes.

We make three modifications to these architectures.

1. We remove the bias from the final classification layer; this helps keep the logits of the different tasks on a similar scale.
2. In the experiments pertaining to Results 4 and 5, we replace batch normalization with layer norm in the Wide-Resnet. This is because we found in preliminary experiments that batch-normalization parameters make training meta-learning models very sensitive to choices of hyper-parameters (e.g., the support or query shot), and that the learned representations of new tasks were quite different in terms of their predictions (and thereby the Bhattacharyya distance) but all the difference was coming from modifications to the BN parameters.
3. In the Resnet-50, we replace the pooling layers with BlurPool (Zhang, 2019). The bias parameter in batch normalization is set to zero with the affine scaling term set to one.

Training procedure All models are trained in mixed-precision (32-bit weights, 16-bit gradients) using stochastic gradient descent (SGD) with Nesterov's acceleration with momentum coefficient set to 0.9 and cosine annealing of the learning rate schedule. Batch-normalization parameters are excluded from weight decay.

CIFAR10 datasets use padding (4 pixels) with random cropping to an image of size 28×28 or 32×32 respectively for data augmentation. CIFAR10 images additionally have random left/right flips for data augmentation. Images are finally normalized to have mean 0.5 and standard deviation 0.25.

Supervised learning models (including fine-tuning) for CIFAR10 are trained for 100 epochs with a batch-size of 64 and weight decay of 10^{-5} using the Wide-Resnet.

Episodic meta-learners are trained using a Wide-Resnet and with the prototypical loss (Snell et al., 2017a). For the 2-way meta-learner, each episode contains 20 query samples and 10 support samples. For the 5-way meta-learner, each episode contains 50 query samples and 10 support samples. We found Result 5 to hold across different choices of these hyper-parameters in small-scale experiments. Models are trained for around 750 epoch and the episodic learner is about 5 times slower to train with respect to wall-clock time.

We train models using SimCLR on CIFAR10 and on tasks created from CIFAR10. For the augmentations, we use random horizontal flips, random grayscale, random resized crop and color jitter. Models are trained for 200 epochs for 2-way classification problems and for 500 epochs when trained on the entirety of CIFAR10 with the Adam optimizer and an initial learning rate of 0.001.

A.1 Experiments on Imagenet

We make use of FFCV (Leclerc et al., 2022). which is a data-loading library that replaces the pytorch Dataloader. FFCV reduces the training time on Imagenet to a few hours, which allows us to train 100s of models on Imagenet, or on tasks created from it. Our implementation of Imagenet training builds on the FFCV repository [1].

Imagenet models are trained for 40 epochs with progressive resizing – the image size is increased from 160 to 224 between the epochs 29 and 34. Models are trained on 4 GPUs with a batch-size of

[1] https://github.com/libffcv/ffcv-imagenet/tree/main/

512. The training uses two types of augmentations – random-resized crop and random horizontal flips. Additionally, we use label smoothing with the smoothing parameter set to 0.1.

A.2 Implementing InPCA in very high dimensions

We calculate an InPCA embedding of models along multiple trajectories, e.g., a typical experiment has about 25 trajectories (multiple random seeds, tasks, or representation learning methods) and about 50 models (checkpoints) along each trajectory. Each model is a very high-dimensional object (with dimensionality NC where $N \sim 10^5$ and $C \sim$ 10-10^3). Even if the matrix D in (9) is relatively small with $n \sim 1250$, each entry of D is $\mathrm{d_B}(P_u, P_v)$ and therefore requires $\sim 10^8$ operations to compute. Implementing InPCA—or even PCA—for such large matrices requires a large amount of RAM. We reduced the severity of this issue to an extent using Numpy's memmap functionality https://numpy.org/doc/stable/reference/generated/numpy.memmap.html. Also note that calculating only the top few eigenvectors of (9) suffices to visualize the models, we do not need to calculate all.

The formula (2) is an effective summary of the discrepancies between how the predictions made by two probabilistic models differ; even small differences in two models, e.g., even if both P_u and P_v make mistakes on exactly the same input samples, if $p_u^n(c)$ is slightly different than $p_v^n(c)$ for even one of n or c, the divergence is non-zero. InPCA is capable of capturing the differences between two such models (9). However, when the number of classes is extremely large, the number of terms in the summation is prohibitively large and analyzing the discrepancies or calculating the embedding becomes rather difficult.

We developed a method to work around this issue. We can use a random stochastic matrix (whose columns sum up to 1) to project the outputs for each sample $\{p_u^n(c)\}_{c=1,\ldots,C}$ into a smaller space before calculating (2). This amounts to pretending as if the model predicts not the actual classes but a random linear combination of the classes (even if the model is trained on the actual classes). This is a practical trick that is necessary only when we are embedding a very large number of very high-dimensional probabilistic models. We checked in our Imagenet experiments that using this trick gives the same embeddings.

In this paper, we did not need to use this projection trick.

B Calculating mean trajectories

We defined the distance between two trajectories to be $\mathrm{d_{traj}}(\tau_u^{1\to \mathrm{U}}, \tau_v^{2\to \mathrm{U}})$, i.e., the integral of the Bhattacharyya distance between the trajectories after mapping them to the same task and re-indexing them using the geodesic. This quantity is key in our work. Say we wish to compare a model trained on two tasks: cats vs. dogs and airplane vs. truck from CIFAR-10. We initialize multiple models for each of these two supervised learning problems (and we do so for every experiment in this paper) and train these 10 models. We can now calculate the mean trajectory of models on a task

$$\operatorname*{argmin}_{\tau_\mu^1} \frac{1}{K} \sum_{k=1}^{K} \mathrm{d_{traj}}(\tau_{u_k}^1, \tau_\mu^1).$$

This optimization problem is very challenging because the variable is a trajectory of probabilistic models in a high-dimensional space. Even if we were to split this minimization and do it independently across time, this is still difficult because the solution is the so-called Bhattacharyya centroid on the product manifold defined in (1) and cannot be computed in closed form. See (Nielsen & Boltz, 2011) for an iterative formula. We therefore simply take the arithmetic mean of the probability distributions, i.e., $P_{\mu(t)} = \frac{1}{K}\sum_{k=1}^{K} P_{w_i(t)}$. This is similar to ensembling. We use the radius of the tube around the mean trajectory, i.e.,

$$r_u = \max_k \mathrm{d_{traj}}(\tau_{u_k}^1, \tau_\mu^1)$$

to normalize distances (more precisely, we normalize using the average of the radii of the two trajectories being compared). Note that this radius depends upon time (and is computed after mapping and reindexing the trajectories). If the distance between the means of two sets of trajectories is smaller than their individual average radii, then the tubes around the means intersect each other. In such cases, one can say that the representations learned (at that time point) are not distinguishable. We next show all distances between reindexed points along the trajectories discussed in Figs. 1, 3 and 4. Note that each curve gives the integrands in (5), not the integral.

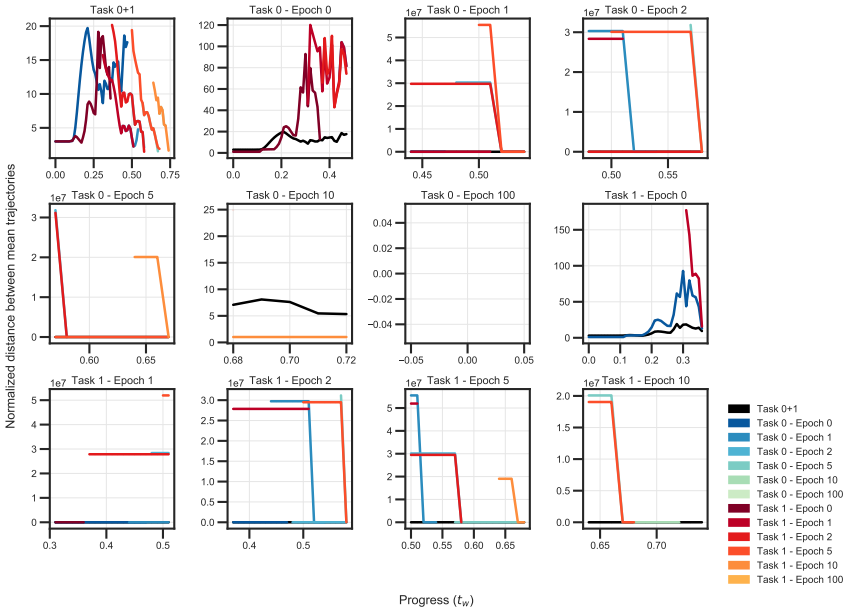

(a)

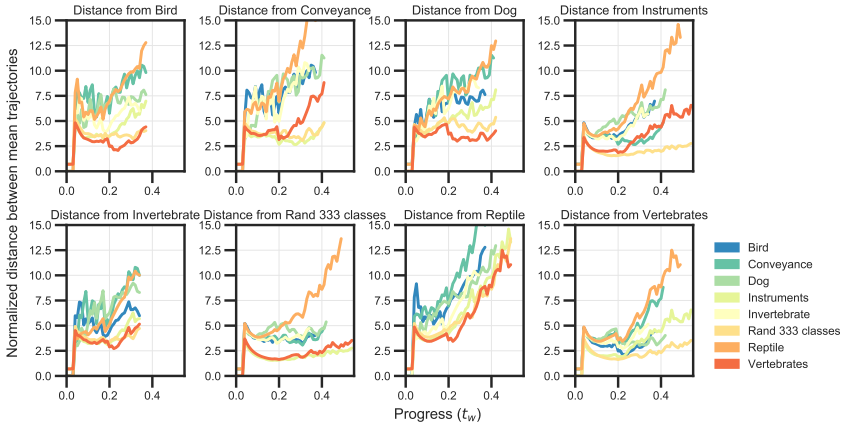

(b)

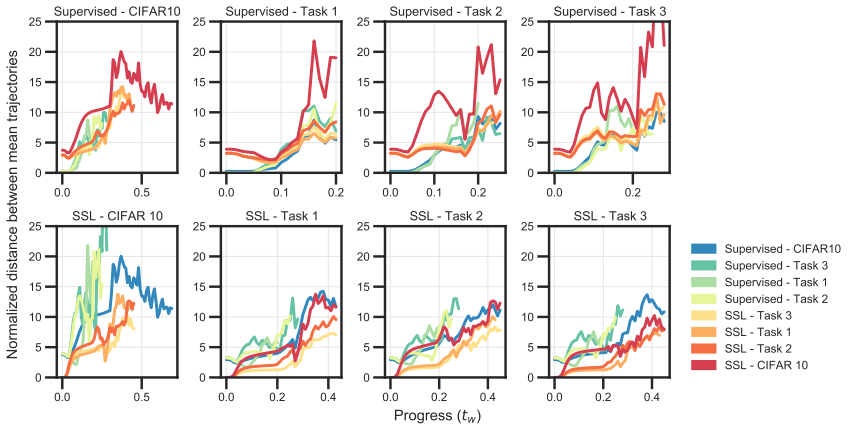

(c)

Figure A1: This figure shows the extended version of the distances between trajectories of probabilistic models; two of them are identical to the ones in Fig. 3b and Fig. 4b.